Ru(II)-Arene Complexes of Curcumin and Bisdesmethoxycurcumin Metabolites

Noemi Pagliaricci,[a] Riccardo Pettinari,[a] Fabio Marchetti,[b] Alessia Tombesi,[a] Sara Pagliaricci,[a] Massimiliano Cuccioloni,[c] Agustín Galindo,[d] Farzaneh Fadaei-Tirani,[e] Mouna Hadiji,[e] Paul J. Dyson.[e]**

[a] School of Pharmacy, [b]School of Science and Technology, and [c]School of Biosciences and Veterinary Medicine, University of Camerino, via Madonna delle Carceri, 62032 Camerino, MC, Italy; [d]Departamento de Química Inorgánica, Facultad de Química, Universidad de Sevilla, 41012 Sevilla, Spain; [e] Institut des Sciences et Ingénierie Chimiques, École Polytechnique Fédérale de Lausanne (EPFL), 1015 Lausanne, Switzerland.

KEYWORDS. Curcumin, Bisdesmethoxycurcumin, Ruthenium complexes, Tetrahydrocurcumin, Bisdesmethoxytetrahydrocurcumin, Bioorganometallic chemistry.

ABSTRACT

In this decades, curcuminoids are attracting much scientific attention as well as their complexes but only little attention was given to their metabolic derivatives. Here the first examples of (arene)Ru(II) complexes with curcuminoid metabolites, tetrahydrocurcumin (THcurcH) and bisdesmethoxytetrahydrocurcumin (THbdcurcH), have been prepared and characterized. The neutral complexes [Ru(arene)(THcurc)Cl] and [Ru(arene)(THbdcurc)Cl] (arene = cymene, benzene or hexamethylbenzene) were characterized by NMR spectroscopy and ESI mass spectrometry, and the crystal structures of three complexes were determined by X-ray diffraction analysis. Compared to curcuminoids, these metabolites lose their conjugated double bond system responsible for their planarity, showing unique *closed* conformation structures. Both *closed* and *open* conformations have been analyzed and rationalized using density functional theory (DFT). The cytotoxicity of the complexes was evaluated *in vitro* against human ovarian carcinoma cells (A2780 and A2780cisR), human breast adenocarcinoma cells (MCF-7 and MCF-7CR), as well as against non- tumorigenic human embryonic kidney cells (HEK293) and human breast (MCF-10A) cells and compared to the free ligands, cisplatin, and RAPTA-C. There is a correlation between cellular uptake and cytotoxicity of the compounds, suggesting that cellular uptake and binding to nuclear DNA may be the major pathway for cytotoxicity. However, the levels of the complexes binding to DNA do not strictly correlate with the cytotoxic potency, indicating that other mechanisms are also involved. In addition, treatment of MCF-7 cells with [Ru(cym)(THcurc)Cl] showed a significant decrease in p62 protein levels, which is generally assumed as a non-cisplatin-like mechanism of action involving autophagy. Hence, a cisplatin- and a non-cisplatin-like concerted mechanism of action, involving both apoptosis and autophagy, is possible.

INTRODUCTION

The turmeric plant (*Curcuma longa*), a perennial herb belonging to the ginger family, is cultivated extensively in south and southeast tropical Asia.[1,2] The main polyphenol constituents of turmeric's rhizome are curcuminoids that have three main chemical components, including curcumin (curcH), desmethoxycurcumin, and bisdemethoxycurcumin (bdcurcH).[3] Recently, interesting results have emerged from clinical studies of curcumin in various pathologies. In particular, positive effects have been observed on inflammation, skin, eye, central nervous system, respiratory, cardiovascular, gastrointestinal, urogenital and metabolic disorders.[4] Curcumin has also shown therapeutic potential in chemoprevention and for the treatment of cancer.[5–7] Although curcuminoids have been successfully evaluated for a wide range of biological activities, they show two main limitations related to the poor bioavailability and rapid metabolism.[8] The metabolism of curcumin in humans produces several products using three main pathways, degradation, O-conjugation and reduction.[9,10] The reduction products are mainly tetrahydrocurcumin (THcurcH) (Scheme 1), hexahydrocurcumin and octahydrocurcumin.[11–13] THcurcH has been reported to show a wide range of therapeutic properties similar to curcumin such as anti-oxidant, radical-scavenging, anti-metastatic and anti-carcinogenic activities, but unlike curcumin, THcurcH has greater bioavailability.[14,15] Having additional hydrogens, THcurcH is more hydrophilic than curcumin[16] and pharmacokinetic assessments reveal that it is more stable than curcumin in phosphate buffers at neutral pH and plasma.[17] Following our recent studies on the anticancer activity of Ru(II) half-sandwich complexes of curcuminoids,[18] we decided to extend our research to the synthesis and characterization of new organometallic Ru(II) complexes containing the more important curcuminoid metabolites, i.e. tetrahydrocurcumin (THcurcH) and bisdesmethoxytetrahydrocurcumin (THbdcurcH).

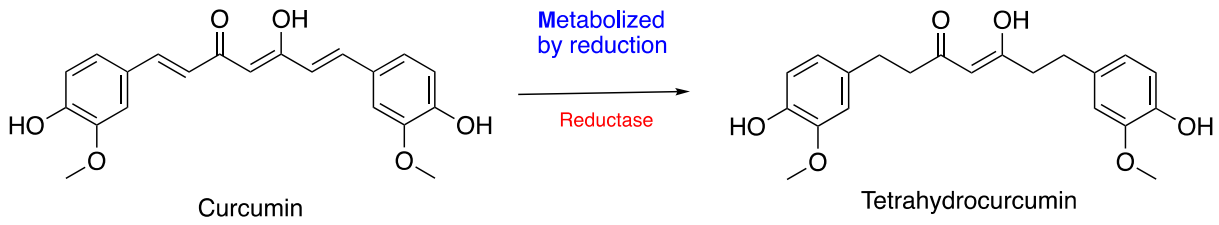

Scheme 1. Tetrahydrocurcumin obtained from curcumin after oral administration following metabolization by enzymatic reduction.

RESULTS AND DISCUSSION

The curcumin metabolite ligands, tetrahydrocurcumin (THcurcH) and tetrahydrobisdemethoxycurcumin (THbdcurcH), were synthesized as reported in Scheme 2, starting from the commercially available curcumin and bisdemethoxycurcumin. Curcumin and bisdemethoxycurcumin were dissolved in methanol and then, the catalyst Pd/$BaSO_4$ was added a to the chilled solution. The reaction mixture was stirred at room temperature for 10 h under H_2 (2 atm). Work up of the reaction mixture and purification by chromatography column gave THcurH and THbdcurc as white powders (77% and 60 % yield, respectively). The IR spectra of the two ligands possess aliphatic C-H absorption in the region of 3066-2841 cm^{-1} and no longer show the typical ν (C=C) vibration around 1590-1530 cm^{-1}, characteristic of the α-β unsaturated chain.

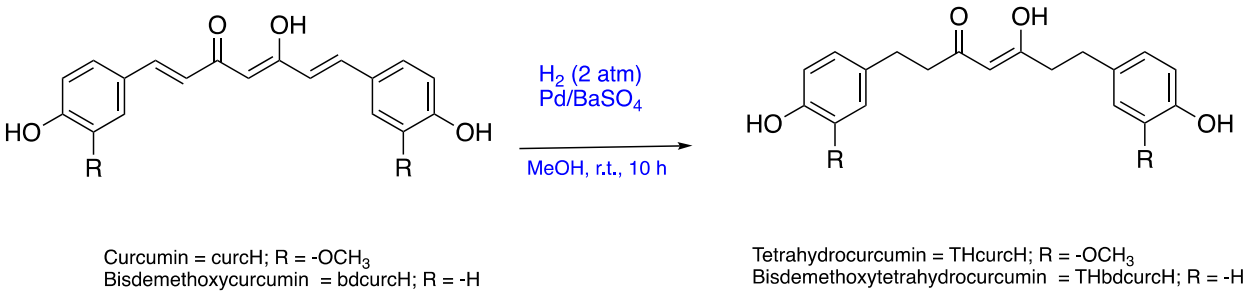

Scheme 2. Synthesis of THcurcH and THbdcurcH.

They were fully characterized by mass spectrometry and ^{1}H, ^{13}C NMR and bidimensional spectroscopy (see Supporting Information). Complexes **1**–**6** were prepared from the reaction of the appropriate dimer, $[Ru(arene)Cl_2]_2$, (arene = cymene, benzene or hexamethylbenzene) with THcurcH and THbdcurcH and potassium hydroxide in methanol (Scheme 3).

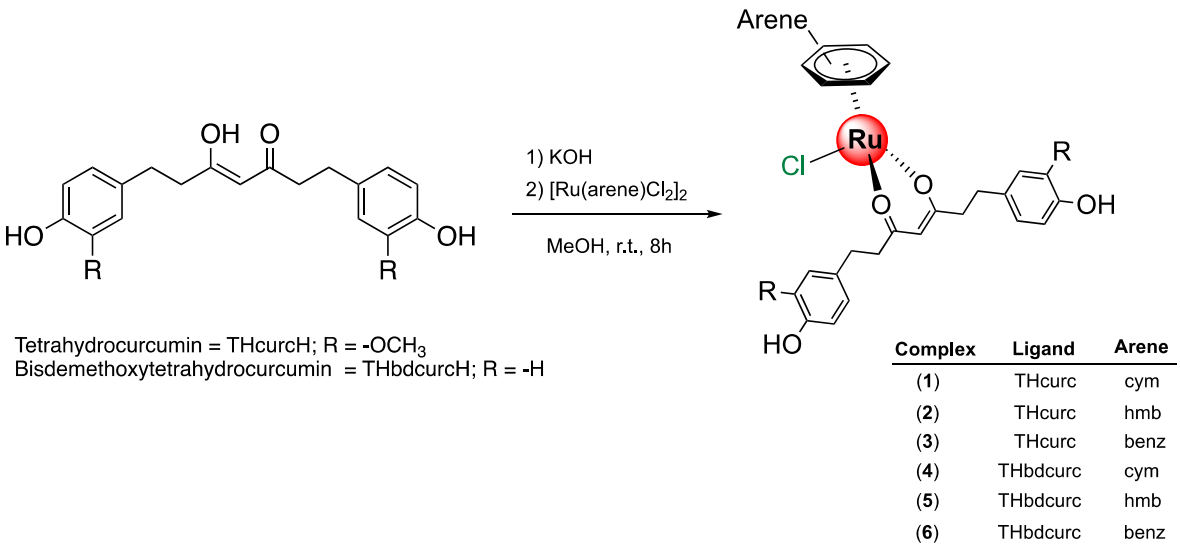

Complex	Ligand	Arene
(**1**)	THcurc	cym
(**2**)	THcurc	hmb
(**3**)	THcurc	benz
(**4**)	THbdcurc	cym
(**5**)	THbdcurc	hmb
(**6**)	THbdcurc	benz

Scheme 3. Synthesis of ruthenium(II)-arene complexes **1-6**.

Complexes **1**–**6** are air-stable and soluble in acetone, acetonitrile, DMSO, chlorinated and alcoholic solvents and are slightly soluble in water. The IR spectra of **1**–**6** show the typical ν(C=O, C=C) bands of THcurc and THbdcurc at lower wavenumbers than the corresponding bands in the free ligands, as a consequence of coordination through both the carbonyl arms to the metal. In the far-IR region, absorptions in the range 230-295 cm^{-1} may be assigned to ν(Ru–Cl) stretches.[19] Electrospray ionization (ESI) mass spectra of **1**–**6** in positive ion mode, recorded in CH_3CN, show the expected isotopic patterns and display peaks that correspond to $[Ru(arene)(THcurc/THbdcurc)]^+$ arising from the dissociation of the chloride ligand. ^{1}H- and ^{13}C-

NMR spectra were assigned based on $^{1}H-^{1}H$ and $^{1}H-^{13}C$ couplings, arising from the bidimensional $\{^{1}H-^{1}H\}$-COSY, $\{^{1}H-^{13}C\}$-HSQC and $\{^{1}H-^{13}C\}$-HMBC experiments. The ^{1}H and ^{13}C NMR spectra of **1**–**6** in $CDCl_3$ and CD_3CN display the expected signals due to the coordinated arene ligands. Furthermore, in tetrahydrocurcumin and bisdesmethoxytetrahydrocurcumin there are diagnostic protons (H1 and H3-3') and carbons (C1, C2-2' and C3-3') which, being closer to the coordination site, are shifted to higher fields compared to those of free ligands (Supporting Information). The stability profile of complexes **1**-**6** and ligands THcurcH and THbdcurcH has been evaluated under physiologically relevant conditions in phosphate-buffered solution (PBS, pH = 7.4). The solutions, with a concentration of about 10^{-6} M, were monitored over time using UV-Visible spectroscopy. The compounds were initially solubilized in DMSO and then diluted to 10% DMSO with PBS. The absorbance spectra were collected after 24, 48 and 72 h. The hydrogenated ligands THcurcH and THbdcurcH were shown to be more stable than their parent unmodified curcuminoids, as expected from the literature.[20,21] The absorbance profile of curcumin (curcH) and bisdemethoxycurcumin (bdcurcH) (Figure S51 **a** and **c**) gradually decrease with time indicating their instability under physiological conditions. In contrast, the reduced ligands THcurcH and THbdcurcH maintain their structure for a longer time with the absorbance profile of THcurcH remaining unchanged over 72 hours and THbdcurcH being stable for at least 48 hours (Figure S51 **b** and **d**). The complexes show good stability with **1**-**3** that contain the THcurc moiety generally being more stable than their analogue with THbdcurc, **4**-**6** (Figure S52). Compound **1** is the most stable for which changes in the absorption spectra were not observed. The least stable complexes are those with a benzene ligand. With the exception of **1**, all complexes show a hypochromism in the maximum absorption intensity at about 270 nm, accompanied by a 3-5 nm red shift after 72 h, presumably due to aquation phenomena derived from the replacement of chloride ligand with a

H_2O molecule. This behavior represents a crucial step in the activation of ruthenium-arene anticancer compounds.[22] The stability of the complexes was also investigated using ^{1}H-NMR spectroscopy (conducted for **1** and **4**). The δ values of the characteristic peaks in all the spectra remained unchanged over 5 days, indicating that the complexes are stable (Figure S48 and S49). However, additional peaks appear in the ^{1}H-NMR spectra of compound **4** which could be due to secondary species formed by the hydrolysis of Ru-Cl bond. Moreover, ^{1}H-NMR spectra of compound **4** recorded in CD_3CN do not show any additional peaks over time (Figure S50).

X-ray crystallography

Complexes **2-4** were structurally characterized by X-ray crystallography (see Experimental). Their structures show the expected piano stool geometry around the Ru(II) center (Figures 1-3). Selected structural parameters are collected in Table S1. The Ru-Cl bond lengths are within the typical 2.40-2.43 Å range, and the Ru-arene centroid distances are close to 1.65 Å as usual in neutral complexes. The THcurc and THbdcurc ligands coordinate the ruthenium center in a similar fashion, with Ru-O distances between 2.06 and 2.09 Å. These values are similar those found for related Ru complexes with curcumin (curc) and bisdemethoxycurcumin (bdcurc) ligands in which this distance is close to 2.06 Å.[23] The curcuminoid metallacycle is delocalized and the C-O distances in **2-4** are around 1.27-1.28 Å, which are longer than those calculated for the localized C=O bonds in the THcurc and THbdcurc precursors (1.24 Å, see Figure S1 and discussion below).

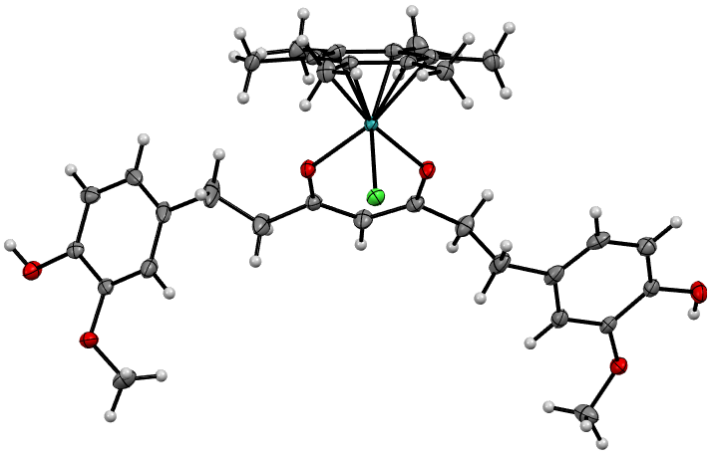

Figure 1. Molecular structure of **2**.

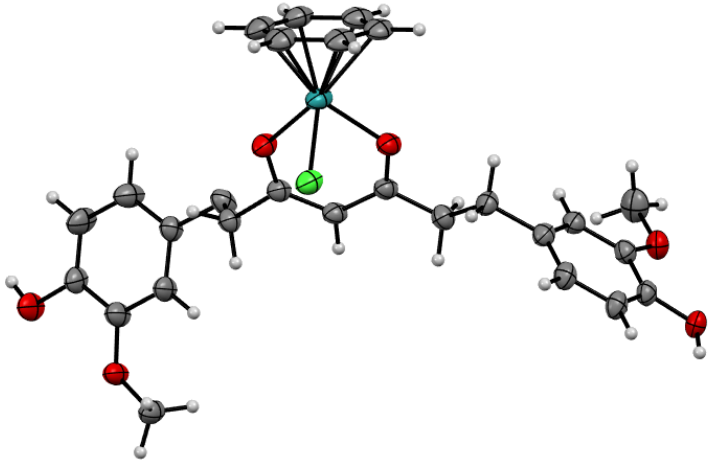

Figure 2. Molecular structure of **3** (CH_2Cl_2 solvate is not shown).

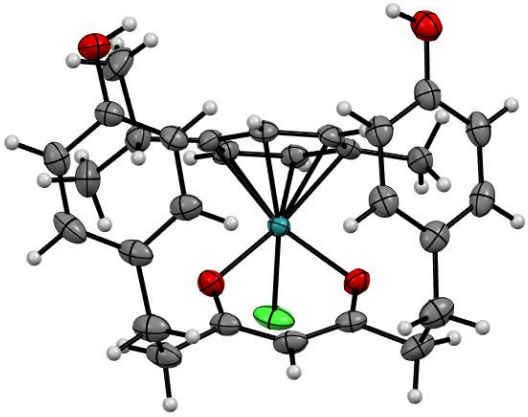

Figure 3. Molecular structure of **4**.

From an inspection of the structures shown in Figures 2-4, the anomalous conformation of the THbdcurc ligand in **4** attracts attention. Whereas the C(O)-CH_2-CH_2-C_{ipso} torsion angles are close to 60º in **4** (*closed* conformation), the same angles for **2** and **3** are close to 168 and 177º, respectively (*open* conformation). For this reason, the 3D crystal packing of **2**-**4** was analyzed. In the crystal of **2**, two types of hydrogen bonds are observed. One is formed between the coordinated chloro ligand and the O-H bond of THcurc. The Ru-Cl···H-O distance of 2.298 Å falls into the region of intermediate hydrogen bonds[24] (Figure S2a). The second are hydrogen bonds formed as a result of a double interaction between the -OH and -OMe substituents of THcurc (Figure S2b), with a Me-O···H-O distance of 2.307 Å. In addition to this hydrogen bonding network, there are additional short contacts of the chloro ligand with two methyl groups of two adjacent molecules (Figure S2c), one from the OMe group of THcurc and the other from a Me group of hexamethylbenzene (hmb). The crystal packing of **3** is built up by a hydrogen bonding network created by interactions between the -OH substituents of THcurc of two adjacent molecules (H-O···H-O distance of 2.043 Å, Figure S3a) and some other weak short contacts between the Ru-Cl moiety and adjacent C-H bonds (see unit cell in Figure S3b). The asymmetric unit of **4** contains two molecules with a π-π stacking interaction between the cymene ligands characterized by a centroid-centroid distance of 3.945 Å (Figure S4a). The presence of two -OH functionalities in the THbdcurc ligand allows the formation of two possible intermolecular Ru-Cl···H-O hydrogen bonds. However, both -OH groups are involved in hydrogen bonding with the same chloro ligand. Figure S4b shows the orientation of the Ru-Cl···H-O hydrogen bonds and additional short contacts of the chloro ligand with C-H bonds of the cymene ligand. All these intermolecular interactions are viable only if a *closed* conformation is attained in the crystal.

Theoretical studies

The proligands THcurcH and THbdcurcH, their anions and ruthenium complexes **1**-**6** were analyzed using density functional theory (DFT) to obtain information about their frontier molecular orbitals (MOs) of the precursors and ligands and about the electronic structure of the complexes. Geometry optimizations were performed with the actual compounds, without symmetry restrictions, and starting from the experimental X-ray coordinates for complexes **2**-**4**. The optimized structures of the THcurcH and THbdcurcH proligands and their anions are collected in Figure S1. Significant differences in the structural parameters of the proligands with respect to the previously reported curcH and bdcurcH proligands are not observed,[1] with the exception of the presence of the C-C double bond. Analysis of the frontier MOs obtained for the THcurc and THbdcurc anions reveals that HOMO-9 and HOMO-10 are the *in-phase* and *out-of-phase* combinations, respectively, of the σ lone pairs of oxygen atoms (Figure S5). These orbitals are primarily responsible for σ-coordination of the ligands to the ruthenium center, although there are also minor contributions from HOMO-1 and HOMO-2 (Figure S5). The topology of these MOs is essentially identical to that calculated for the anions curc and bdcurc (not shown).[25] Even their energies are quite similar and, consequently, no major differences between unsaturated and saturated curcuminoid ligands are expected when bonded to the Ru center (see below).

The optimized structures of the complexes are shown in Figure 4, with selected structural parameters collected in Table S2. As previously reported in DFT studies of related Ru systems,[25] [26] the selected combination of method and basis sets provides a satisfactory structural description of these complexes. A comparison of the structural parameters of **2**-**4** with those determined by X-ray diffraction is good (see Table S1). The exception is the bond distance from the Ru ion to the arene centroid, which is always slightly overestimated, as noted previously in similar Ru-arene

complexes.[23,25,26] The calculated IR spectra of **1-6** confirm the IR assignments. For instance, the symmetrical ν(C-O) stretching calculated at around 1570 cm^{-1} and the ν(Ru-Cl) stretching calculated at around 266 cm^{-1} (see Table S1B).

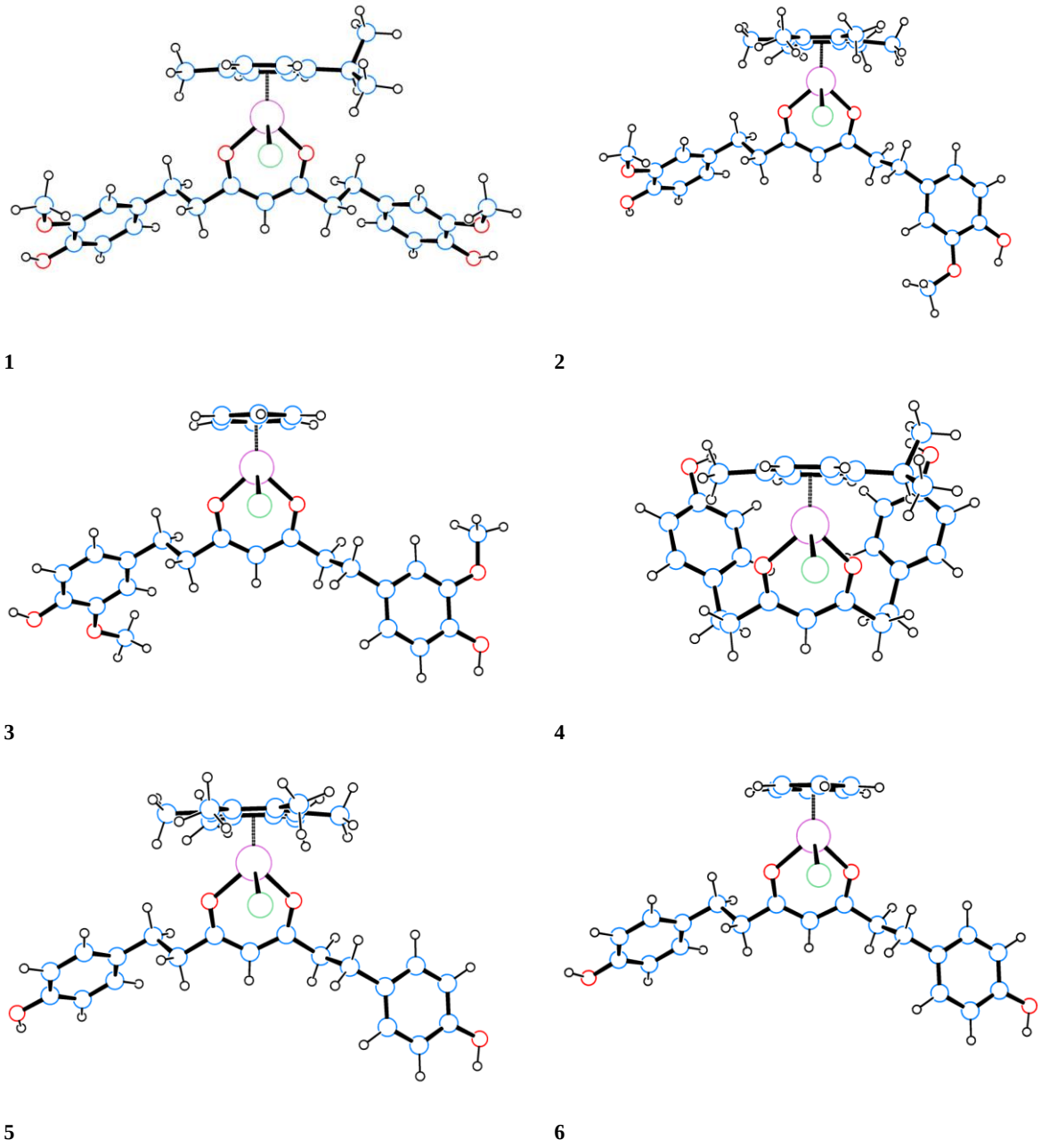

Figure 4. Optimized structures of **1-6**.

As evident from Figure 4, the optimized structure of **4** with a *closed* conformation is different from the other structures and was obtained by an optimization starting from the crystallographic coordinates. To identify whether the *open* conformation of **4** is more stable, both the *closed* and *open* conformations of complexes **1**-**6** were calculated in gas phase without intermolecular interactions. The resulting optimized structures of the conformers, not shown in Figure 4, are displayed in Figure S6. The open conformation is always the most stable with relative ΔG energy differences within the range of 1.3-11.9 kcal/mol (Table S3). The energy differences are higher for THcurc than for THbdcurc ligand and the lowest difference is found for the less sterically demanding benzene ligand. In any case, the closed conformation of THbdcurc found in the crystal structure of **4** is due to the presence of intermolecular interactions in the solid state. The hydrogen bonds and π-π stacking interactions counterbalance the energy difference between both conformations. An investigation of compound **4** by{^{1}H-^{1}H}-NOESY NMR spectroscopy in acetonitrile at 25, 0 and -25 °C (Figures S53a-c, respectively) confirmed the *open* conformation suggested by DFT calculations carried out in the gas phase. In fact, cross-coupling interactions between cymene and bisdesmethoxytetrahydrocurcumin of the *closed* conformation found in the solid state were not observed in CD_3CN solution.

With the aim of comparing the behavior of THcurc and THbdcurc as ligands in **1**-**6** with their curc and bdcurc analogues, complexes **7**-**12** were additionally calculated, at the same theoretical level. In these complexes, the THcurc and THbdcurc ligands were replaced by curc and bdcurc, respectively. Their optimized structures are shown in Figure S7, and selected structural parameters are collected in Table S4. The presence of the C-C double bond in curc and bdcurc ligands of complexes **7**-**12** excludes the possibility of ligand conformations. To compare the bonding capabilities of these ligands, the Mayer indexes of the Ru-O bonds were calculated for all

derivatives **1**-**12** (see Table S5). No significant differences were found between the two types of ligands with respect to the coordination to ruthenium. Only minor differences were encountered in the C-O bonds, where lower Mayer indexes were calculated for curc and bdcurc than for THcurc and THbdcur, in agreement with the slightly longer C-O distances (around 1.284 Å) in **7**-**12** with respect to those of **1**-**6**.

Cytotoxicity studies

To assess the cytotoxicity of the compounds, the MTT assay was performed using human ovarian carcinoma cell line (A2780) and its cisplatin resistant form (A2780cisR), human breast adenocarcinoma cells (MCF-7) and its cisplatin resistant counterpart (MCF-7CR), as well as against non-tumorous human embryonic kidney cells (HEK293) and human breast (MCF-10A) cells over an incubation period of 72 h. The resulting IC_{50} values are presented THbdcurcH has one of the best selectivity profiles as it appears to be inactive on the human embryonic cell line HEK293T (IC_{50} > 100 µM) while having one of the lowest IC_{50} values of 56 ± 10 µM on the A2780 cells. Among the studied complexes, **2** is the most potent on all tested cell lines, followed by **1** which has a notable selectivity on the HEK293T cell line with an IC_{50} of 72 ± 16 µM compared to 47 ± 8 µM on the A2780 cell line. Despite having a lower cytotoxicity on the ovarian cancer cell line, complexes **3** and **4** are inactive on the HEK293T cells (IC_{50} > 100 µM), conferring them with a higher selectivity than **5** and **6**. Conversely, with the exception of the benzene derivatives **3** and **6**, complexation of THcurc and THbdcurc to the Ru(II)-arene unit dramatically increases the cytotoxicity toward MCF-7 breast cancer cells, with **1** and **2** in particular displaying IC_{50} values in the low micromolar range (8.0 ± 3.9 and 8.5 ± 1.6, respectively). In MCF-7CR cells, with the acquired resistance to cisplatin, the cytotoxicity of the complexes is partially reduced,

supporting the notion that both cisplatin-like and non-cisplatin-like mechanisms of action may be at play.

Table 1.

THbdcurcH has one of the best selectivity profiles as it appears to be inactive on the human embryonic cell line HEK293T (IC_{50} > 100 µM) while having one of the lowest IC_{50} values of 56 ± 10 µM on the A2780 cells. Among the studied complexes, **2** is the most potent on all tested cell lines, followed by **1** which has a notable selectivity on the HEK293T cell line with an IC_{50} of 72 ± 16 µM compared to 47 ± 8 µM on the A2780 cell line. Despite having a lower cytotoxicity on the ovarian cancer cell line, complexes **3** and **4** are inactive on the HEK293T cells (IC_{50} > 100 µM), conferring them with a higher selectivity than **5** and **6**. Conversely, with the exception of the benzene derivatives **3** and **6**, complexation of THcurc and THbdcurc to the Ru(II)-arene unit dramatically increases the cytotoxicity toward MCF-7 breast cancer cells, with **1** and **2** in particular displaying IC_{50} values in the low micromolar range (8.0 ± 3.9 and 8.5 ± 1.6, respectively). In MCF-7CR cells, with the acquired resistance to cisplatin, the cytotoxicity of the complexes is partially reduced, supporting the notion that both cisplatin-like and non-cisplatin-like mechanisms of action may be at play.

Table 1: IC_{50} values in µM of THcurcH, THbdcurH, complexes **1-6**, cisplatin and RAPTA-C on cisplatin sensitive and resistant human ovarian carcinoma (A2780 and A2780cisR), human embryonic kidney (HEK293T), cisplatin sensitive and resistant breast adenocarcinoma (MCF-7 and MCF-7CR), and epithelial normal breast cells (MCF-10A). Values are given as the mean obtained from 3 independent experiments ± standard deviation. The derivative curcumin ligands, THcurcH and THbdcurcH, display a similar and moderate toxicity on the ovarian cancer cell lines A2780 and A2780cis with IC_{50} values around 50 µM.

	A2780	**A2780cisR**	**HEK293T**	**MCF-7**	**MCF7CR**	**MCF10A**
THcurcH	57 ± 30	56 ± 25	82 ± 27	>100	>100	44 ± 13

THbdcurcH	56 ± 10	51 ± 10	>100	50 ± 9.2	>100	47 ± 16
1	47 ± 8	64 ± 18	72 ± 16	8.0 ± 3.9	19 ± 2	6.2 ± 1.7
2	26 ± 3	32 ± 3	32 ± 10	8.5 ± 1.6	19 ± 7	7.5 ± 1.6
3	74 ± 14	72 ± 13	>100	>100	>100	>100
4	77 ± 19	>100	>100	57 ± 2	29 ± 9	33.6 ± 7
5	72 ± 17	86 ± 17	70 ± 29	20 ± 7	37 ± 6	17 ± 7
6	64 ± 8	72 ± 8	88 ± 3	>100	>100	98 ± 9
cisplatin	1.1 ± 0.6	9.0 ± 3.5	3.0 ± 1.1	4.2 ± 2.3	49 ± 7	12 ± 4
RAPTA-C	>100	>100	>100	>100	>100	>100

Cellular Uptake

In order to investigate a possible relationship between the structure of the complexes and the observed cytotoxicity, the uptake of complexes **1**-**6** in MCF-7 cells was studied using fluorescence anisotropy measurements within 2 hours. In general, we observed three different internalization behavior over the time-frame. Specifically, the free ligand THbdcurcH and **2**, **4** and **5** showed a comparable three-stage internalization mode (membrane entry, permanence in the membrane and intracellular release), but with significant differences in individual entry and release rates (k_{in} and k_{out} values found in Table 2). Complexes **1** and **6** were retained for a longer time in the membranes, with no evidence of release during the first 2 h. Conversely, the internalization of ligand THcurcH and complex **3** involve a peculiar mechanism which does not follow the mono-exponential models described in the Experimental section (Figure S54).

The ruthenium complexes show faster cellular uptake compared to THcurcH and THbdcurcH (Table 2). Quantitative analysis of the internalization kinetics showed a direct correlation between the rate membrane entry with the cytotoxicity observed toward MCF-7 cells, with higher values

of k_{in} (i.e., faster membrane entry) displayed by **1** and **4** (cymene) and **2** and **5** (hexamethylbenzene), which are associated with a higher cytotoxicity. Complexes **3** and **6** (benzene) showed slower or even not observable values of k_{in}, consistent with their lower cytotoxicity.

Table 2. Kinetic parameters for membrane entry and exit events.

	k_{in} ($M^{-1}s^{-1}$)	k_{out} (s^{-1})	IC_{50} *MCF-7*
THcurcH	n.o.	n.o.	>100
[Ru(cym)(THcurc)Cl] (1)	0.105 ± 0.01	n.o.	8.0 ± 3.9
[Ru(hmb)(THcurc)Cl] (2)	0.158 ± 0.02	0.012 ± 0.003	8.5 ± 1.6
[Ru(benz)(THcurc)Cl] (3)	n.o.	n.o.	>100
THbdcurcH	0.102 ± 0.01	0.023 ± 0.005	50 ± 9.2
[Ru(cym)(THbdcurc)Cl] (4)	0.156 ± 0.02	0.052 ± 0.002	57 ± 2
[Ru(hmb)(THbdcurc)Cl] (5)	0.133 ± 0.02	0.048 ± 0.002	20 ± 7
[Ru(benz)(THbdcurc)Cl] (6)	0.063 ± 0.01	n.o.	>100

DNA Binding

DNA is one of the most important biomolecules in living cells and it represents the primary target for metal-based anticancer agents, with the formation of drug-DNA adducts being an established apoptosis-triggering event.[27] Here, the ds-DNA oligomer (3′-CCACCCACTACCCTGGTTGGATGCTAATGT-5′) binding ability of THcurcH, THbdcurcH, and complexes **1**-**6** was kinetically characterized using a standard biosensor-based approach, and the binding modes were further explored both spectrophoto-fluorometrically and by molecular docking studies. The compounds of interest showed low-to-moderate affinity for ds-DNA,[28] with equilibrium dissociation constants in the submillimolar-to-micromolar range (Table S8), only THcurcH, **1**, **3** and **4** showing similar affinity for ds-DNA compared with other previously tested

Ru compounds.[29] All binding events followed mono-exponential binding kinetics (Figures S55a and b), compatible with the ability of the compounds to target ds-DNA on a single site, i.e. the minor groove (Table S9 and Figure S56). There is no clear correlation between the binding to DNA and the cytotoxicity of the compounds.

Quantification of p62 expression levels

In the absence of a correlation between the observed cytotoxicity and the DNA affinity, we evaluated the effects of the treatment on the expression levels of a protein biomarker, namely p62/sequestosome1, which is a multifunctional ubiquitinated binding protein and it is involved in signaling pathways of many cell life activities, including autophagy, and its abnormal expression and regulation are closely associated with development and progression of malignant tumors and mostly associated with breast cancer.[30] In particular, p62 can be degraded in autophagolysosomes, and its expression levels correlate inversely with the autophagic activity.[31] Accordingly, we evaluated the effects of complex **1** (the most cytotoxic compound of the series) and the related parent ligand, THcurcH, on p62 expression. In line with the activation of the autophagic flux, a significant decrease of the levels of p62 protein was observed in MCF-7 cells, this effect being more evident for complex **1**, consistently with its higher cytotoxicity compared to THcurcH (Figure 5).

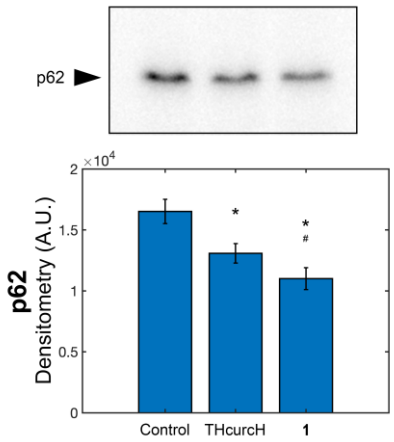

Figure 5. Autoradiographs and densitometric analyses of p62/SQSTM1 levels (A) in MCF7 cells after treatment with 5 μM of complex **1** for 24 h (*$p < 0.01$ compared with the control; $^{\#}p < 0.01$ compared with THcurcH).

CONCLUSIONS

We have reported the first examples of ruthenium(II)-arene complexes containing two curcuminoid metabolites, i.e. THcurc and THbdcurc. The complexes were fully characterized in solution and in the solid-state, with the X-ray structures obtained confirming that the THcurc and THbdcurc ligands coordinate the ruthenium center without significant differences between them and with respect to those found for related Ru complexes with curc and bdcurc. However, an unprecedent *closed* conformation of the THbdcurc ligand was found in **4,** where both -OH groups are involved in intermolecular hydrogen bonding with the same chloro ligand. Both *closed* and *open* conformations were analyzed in gas phase by DFT studies which showed that the *open* conformation is the most stable. Hence, the *closed* conformation of THbdcurc found in the crystal of **4** may be attributed to the presence of intermolecular interactions in the solid state. Interestingly, the arene ligand plays an important role in cell internalization process of the complexes, which in turn contributes to their cytotoxicity. Complexes bearing cymene (**1** and **4**) or hexamethylbenzene

(**2** and **5**) displayed faster uptake into MCF-7 cells, and they also showed higher cytotoxicity than **3** and **6** bearing benzene. Moreover, the difference in cytotoxicity observed between MCF-7 and the cisplatin-resistant counterpart (MCF-7CR) was likely attributable to a concerted cisplatin-like and non-cisplatin-like mechanism of action that involves both apoptosis and autophagy, in line with the ability of the complexes to bind to ds-DNA and to lower the intracellular levels of p62/SQSTM1, respectively.

EXPERIMENTAL SECTION

Materials and Methods

Curcumin and bisdemethoxycurcumin were purchased from TCI Europe and were used as received. All other reagents and solvents were purchased from Aldrich and used as received without further purification. All reactions for the syntheses of proligands and the corresponding ruthenium complexes were carried out in the air. The samples for microanalyses were dried in vacuo to constant weight (35 °C, ca. 0.1 Torr). Elemental analyses (C, H, N) were performed in-house with a Fisons Instruments 1108 CHNS-O Elemental Analyser. IR spectra were recorded on a Perkin-Elmer Frontier FT-IR instrument. ^{1}H and ^{13}C NMR spectra were recorded on a 500 Bruker Ascend (500 MHz for ^{1}H, 125 MHz for ^{13}C) instrument operating at room temperature relative to TMS. Positive ion electrospray mass spectra were obtained on a Series 1100 MSI detector HP spectrometer, using acetonitrile as solvent for all complexes 1-5. Solutions (3 mg/mL) for electrospray ionization mass spectrometry (ESI-MS) were prepared using reagent-grade methanol. Masses and intensities were compared to those calculated using IsoPro Isotopic Abundance Simulator, version 2.1.28. Melting points were recorded on a STMP3 Stuart scientific instrument and on a capillary apparatus. Samples for microanalysis were dried in vacuo to constant weight

(20°C, ca. 0.1 Torr) and analyzed on a Fisons Instruments 1108 CHNS-O elemental analyzer. Uv-stability studies have been conducted with a Varian Caryl spectrometer.

Synthesis of ligands and complexes

THcurcH (1,7-bis(4-hydroxy-3-methoxyphenyl)heptane-3,5-dione)

Curcumin (curcH, 500 mg, 1.4 mmol) was dissolved in CH_3OH (25 mL) and $Pd/BaSO_4$ (50 mg) added. After 10 h agitation under a H_2 atmosphere (2 atm) the reaction mixture was filtered and the remaining oil purified using column chromatography (cyclohexane: ethylacetate, 60:40) to obtain the ligand THcurcH as white powder, yield 78%. It is completely soluble in CH_3OH, CH_3CN, DMSO and CH_3Cl and insoluble in H_2O and hexane. Anal. Calcd. for $C_{21}H_{24}O_6$: C, 67.73, H, 6.50. Found: C, 67.94; H, 6.78. m.p. 87-90 °C. IR (cm^{-1}): 3407 mbr ν(-OH); 3064 w, 3023 w, 3004 w, 2961 w, 2933 m, 2844 w ν(aliphatic C-H); 1702 w, 1601 mbr ν(-C=O); 1450 m, 1429 m. ^{1}H-NMR ($CDCl_3$, 293 K): δ 2.55 (t, 4H, C(3-3')*H*), 2.85 (t, 4H, C(4-4')*H*), 3.86 (s, 6H, -OCH_3), 5.43 (s, 1H, C(1)*H*), 5.51 (sbr, 2H, -O*H*), 6.69 (m, 4H, C(6-6') and C(10-10')), 6.85 (d, 2H, C(9-9')*H*). ^{13}C{^{1}H}-NMR ($CDCl_3$, 293 K): δ 31.31 [s, C(4-4')], 40.37 [s, C(3-3')], 55.88 [s, -O*C*H_3], 99.79 (s, C1), 110.97 [s, C(6-6')], 114.35 [s, C(9-9')], 120.83 [s, C(10-10')], 132.57 [s, C(5-5')], 144.04 [s, C(7-7')], 146.44 [s, C(8-8')], 193.20 [s, C(2-2')]. ESI-MS (-) CH_3CN (m/z [relative intensity, %]): 371 [100] $[(THcurc)]^-$.

THbdcurcH (1,7-bis(4-hydroxyphenyl)heptane-3,5-dione)

THbdcurcH was synthesized as reported for THcurH starting from bisdesmethoxycurcumin (bdcurcH, 500 mg, 1.6 mmol). The ligand was obtained as white powder, yield 60%. It is completely soluble in CH_3OH, CH_3CN, DMSO and CH_3Cl and insoluble in H_2O and hexane. Anal. Calcd. For $C_{19}H_{20}O_4$: C, 73.06; H, 6.45. Found: C, 72.52; H, 6.53. m.p. 105-107 °C. IR (cm^{-1}):

3270 mbr ν(-OH); 3024 w, 2963 sh, 2930 w, 2859 w ν(aliphatic C-H); 1072 w; 1629 sh, 1614 m, 1602 m ν(-C=O); 1514 vs, 1462 m.^{1}H-NMR (CD_3CN, 293 K): δ 2.56 (t, 4H, C(3-3')*H*), 2.81 (t, 4H, C(4-4')*H*), 5.60 (s, 1H, C(1)*H*), 6.73 (m, 4H, C(7-7')*H*), 7.05 (m, 4H, C(6-6')*H*).^{13}C{^{1}H}-NMR (CD_3CN, 293 K): δ 30.28 [s, C(4-4')], 39.74 [s, C(3-3')], 99.51 [s, C(1)], 115.08 [s, C(7-7')], 129.33 [s, C(6-6')], 155.17 [s, C8-8')] 193.73 [s, C(5-5')], 204.28 [s, C(2-2')]. ESI-MS (-) CH_3CN (m/z [relative intensity, %]): 311 [100] $[(THbdcurc)]^-$.

[Ru(cym)(THcurc)Cl] (1)

THcurcH (74 mg, 0.2 mmol) and KOH (11 mg, 0.2 mmol) were dissolved in CH_3OH (5 mL). After 1 h stirring at room temperature, $[Ru(cymene)Cl_2]_2$ (61 mg, 0.1 mmol) was added. The resulting solution was stirred at room temperature for 6 h, after which the solvent was removed under vacuum. The KCl salt was precipitated in a CH_2Cl_2 solution and **1** formed by adding n-hexane. The yellow precipitate (60 mg, 0.093 mmol, yield 93%) was filtered and characterized. It is completely soluble in CH_3OH, CH_3CN, DMSO and CH_3Cl, it is partly soluble in H_2O and insoluble in hexane. Anal. Calcd. for $C_{31}H_{37}ClO_6Ru$: C, 57.98; H, 5.81. Found: C, 56.63; H, 5.67. mp: 135-138 °C. IR (cm^{-1}): IR (cm^{-1}): 3401 mbr ν(-OH); 3068 w, 2967 w, 2919 w, 2850 w ν(aliphatic C-H); 1557 m ν(-C=O); 1514 m; 287 ν(Ru-Cl). ^{1}H-NMR ($CDCl_3$, 293 K): δ 1.31 (d, 6H, -CH(C*H*$_3$)$_2$ of cym, ^{3}J = 7 Hz), 2.22 (s, 3H, -C*H*$_3$ of cym), 2.51 (t, 4H, C3-3'*H*)), 2.84 (m, 5H, C(4-4')*H* and C*H*$(CH_3)_2$ of cym), 3.90 (s, 6H, -OC*H*$_3$), 5.15 (s, 1H, C(1)*H*),5.13 d, 5.38 d (4H, AA′BB′ system, CH_3-C$_6$*H*$_4$-CH$(CH_3)_2$ of cym, ^{3}J = 6 Hz), 5.51 (sbr, 2H, -O*H*), 6.69 (d, 2H, C(10-10')*H*, $^{3}J_{trans}$ = 8 Hz), 6.74 (s, 2H, (C-6-6')*H*), 6.85 (d, 2H, C(9-9')*H*, $^{3}J_{trans}$ = 8 Hz).^{13}C{^{1}H}-NMR ($CDCl_3$, 293 K): δ 17.84 (s, -*C*H_3 of cym), 22.29 (s, -CH(*C*H_3)$_2$ of cym), 30.67 [s, *C*H$(CH_3)_2$ of cym], 32.50 [s, C(4-4')], 42.41 [s, C(3-3')], 56.03 (s, -O*C*H_3), 70.78 [s, C(b-b')], 82.81 [s, C(a-a')], 97.33 (s, Ci'), 98.01 (s, C1), 99.37 (s, Ci), 111.19 [s, C(6-6')], 114.06 [s, C(9-9')], 120.79 [s,

C(10-10')], 133.50 [s, C(5-5')], 143.84 [s, C(8-8')], 146.38 [s, C(7-7')], 188.54 [s, C(2-2')=O]. ESI-MS (+) CH_3CN (m/z [relative intensity, %]): 607 [100] $[Ru(cym)(THcurc)]^+$.

[Ru(hmb)(THcurc)Cl] (2)

THcurcH (74 mg, 0.2 mmol) and KOH (11 mg, 0.2 mmol) were dissolved in CH_3OH (5 mL). After 1 h stirring at room temperature, $[Ru(hexamethylbenzene)Cl_2]_2$ (67 mg, 0.1 mmol) was added. The resulting solution was stirred at room temperature for 6 h, after which the solvent was removed under vacuum. The KCl salt was precipitated in a CH_2Cl_2 solution and **3** crystallized by adding n-hexane. The yellow precipitate (40 mg, 0.060 mmol, yield 60%) was filtered and characterized. It is completely soluble in in CH_3OH, CH_3CN, DMSO and CH_3Cl, it is partly soluble in H_2O and insoluble in hexane. Anal. Calcd. for $C_{33}H_{41}ClO_6Ru$: C, 59.14; H, 6.17. Found: C, 59.04; H,.6.29. mp: 217-219 °C. IR (cm^{-1}): 3278 mbr ν(-OH); 3004 w, 2960 w, 2931 w, 2856 w ν(aliphatic C-H); 1599 w; 1569 vs ν(-C=O); 1513 sbr; 295 ν(Ru-Cl). ^{1}H-NMR ($CDCl_3$, 293 K): δ 2.06 (s, 18H, -(CH_3)$_6$ of hmb), 2.50 (m, 4H, C(3-3')*H*)), 2.79 m, 2.98 m, (4H, C(4-4')*H*), 3.90 (s, 6H, -OCH_3), 5.10 (s, 1H, C(1)*H*), 5.49 (sbr, 2H, -O*H*), 6.70 (d, 2H, C(10-10')*H*, $^3J_{trans}$ = 8 Hz), 6.74 (s, 2H, (C-6-6')*H*), 6.84 (d, 2H, C(9-9')*H*, $^3J_{trans}$ = 8 Hz).^{13}C{^{1}H}-NMR ($CDCl_3$, 293 K): δ 15.03 (s, -(CH_3)$_6$ of hmb), 32.50 [s, C(4-4')], 42.58 [s, C(3-3')], 56.05 (s, -OCH_3), 89.94 [s, C_6 of hmb], 97.64 (s, C1), 111.14 [s, C(6-6')], 114.10 [s, C(9-9')], 120.76 [s, C(10-10'), 133.57 [s, C(5-5')], 143.81 [s, C(8-8')], 146.41 [s, C(7-7')], 188.07 [s, C(2-2')=O]. ESI-MS (+) CH_3CN (m/z [relative intensity, %]): 635 [100] $[Ru(hmb)(THcurc)]^+$.

[Ru(benzene)(THcurc)Cl] (3)

THcurcH (74 mg, 0.2 mmol) and KOH (11 mg, 0.2 mmol) were dissolved in CH_3OH (5 mL). After 1 h stirring at room temperature, $[Ru(benzene)Cl_2]_2$ (50 mg, 0.1 mmol) was added. The resulting solution was stirred at room temperature for 6 h, after which the solvent was removed under

vacuum. The KCl salt was precipitated in a CH_2Cl_2 solution and **5** crystallized by adding n-hexane. The red precipitate (20 mg, 0.034 mmol, yield 34%) was filtered and characterized. It is completely soluble in in CH_3OH, CH_3CN, DMSO and CH_3Cl, it is partly soluble in H_2O and insoluble in hexane. Anal. Calcd. for $C_{27}H_{29}ClO_6Ru$: C, 55.34; H, 4.99. Found: C, 55.34; H, 4.99. mp: 101-104 °C. IR (cm^{-1}): 3414 mbr ν(-OH); 3071 w, 2963 w, 2934 w, 2845 ν(aliphatic C-H); 1614 sh, 1601 w; 1563 m, 1558 m ν(-C=O); 1514 sbr, 1506 s; 266 ν(Ru-Cl). ^{1}H-NMR ($CDCl_3$, 293 K): 2.53 (t, 4H, C(3-3')*H*)), 2.85 (m, 4H, C(4-4')*H*), 3.90 (s, 6H, -OCH_3), 5.17 (s, 1H, C(1)*H*), 5.32 (sbr, 2H, -O*H*), 5.50 (s, 6H, C_6H_6 of benzene), 6.69 (d, 2H, C(10-10')*H*, $^3J_{trans}$ = 8 Hz), 6.75 (s, 2H, (C-6-6')*H*), 6.85 (d, 2H, C(9-9')*H*, $^3J_{trans}$ = 8 Hz).^{13}C{^{1}H}-NMR ($CDCl_3$, 293 K): δ 32.74 [s, C(4-4')], 42.38 [s, C(3-3')], 56.06 (s, -O*C*H_3), 82.26 (s, *C*$_6H_6$ of benzene), 98.22 (s, C1), 111.31 [s, C(6-6')], 114.01 [s, C(9-9')], 120.86 [s, C(10-10'), 133.37 [s, C(5-5')], 143.88 [s, C(8-8')], 146.34 [s, C(7-7')], 188.82 [s, C(2-2')=O]. ESI-MS (+) CH_3CN (m/z [relative intensity, %]): 551 [100] [Ru(benzene)(THcurc)]$^+$.

[Ru(cym)(THbdcurc)Cl] (4)

THbdcurc (62 mg, 0.2 mmol) and KOH (11 mg, 0.2 mmol) were dissolved in CH_3OH (5 mL). After 1 h stirring at room temperature, [Ru(cymene)Cl_2]$_2$ (61 mg, 0.1 mmol) was added. The resulting solution was stirred at room temperature for 6 h, after which the solvent was removed under vacuum. The KCl salt was precipitated in a CH_2Cl_2 solution and **2** crystallized by adding n-hexane. The yellow precipitate (40 mg, 0.069 mmol, yield 70%) was filtered and characterized. It is completely soluble in in CH_3OH, CH_3CN, DMSO and CH_3Cl, it is partly soluble in H_2O and insoluble in hexane. Anal. Calcd. for $C_{29}H_{33}ClO_4Ru$: C,59.84; H, 5.71. Found: C, 60.06; H, 5.59. mp: 195-197 °C. IR (cm^{-1}): 3406 mbr ν(-OH); 3069 w, 2963 m, 2923 m, 2875 w, 2856 w ν(aliphatic C-H); 1613 m ν(-C=O); 1592 m, 1564 vs; 294 ν(Ru-Cl). ^{1}H-NMR (CD_3CN, 293 K): δ

1.26 (d, 6H, CH(C*H*$_3$)$_2$ of cym, ^{3}J = 7 Hz), 2.10 (s, 3H, -C*H*$_3$ of cym), 2.41 (m, 4H, C(3-3')), 2.70 (m, 1H, C*H*(CH$_3$)$_2$ of cym), 2.81 (m, 4H, C(4-4')), 5.10 d, 5.34 d (4H, AA′BB′ system, CH$_3$-C$_6$*H*$_4$-CH(CH$_3$)$_2$ of cym, ^{3}J = 6 Hz), 5.17 (s, 1H, C(1)*H*), 6.77 (d, 4H, C(7, 7')*H*, ^{3}J$_{trans}$ = 8 Hz), 6.89 (sbr, 2H, -O*H*), 7.07 (d, 4H, C(6-6')*H*, ^{3}J$_{trans}$ = 8 Hz). ^{13}C{^{1}H}-NMR (CD$_3$CN, 293 K): δ 16.91 (s, -*C*H$_3$ of cym), 21.42 (s, -CH(*C*H$_3$)$_2$ of cym), 30.37 (s, *C*H(CH$_3$)$_2$ of cym), 31.52 [s, C(4-4')], 41.95 [s, C(3-3')], 78.94 [s, C(b-b')], 82.46 [s, C(a-a')], 96.71 (s, Ci'), 97.62 (s, C1), 99.23 (s, Ci), 114.98 [s, C(7-7')], 129.41 [s, C(6-6')], 132.71 [s, C(5-5')], 155.13 [s, C(8-8')], 188.17 [s, C(2-2')=O]. ESI-MS (+) CH$_3$CN (m/z [relative intensity, %]): 547 [100] [Ru(cym)(THbdcurc)]$^+$.

[Ru(hmb)(THbdcurc)Cl] (5)

THbdcurc (62 mg, 0.2 mmol) and KOH (11 mg, 0.2 mmol) were dissolved in CH$_3$OH (5 mL). After 1 h stirring at room temperature, [Ru(hexamethylbenzene)Cl$_2$]$_2$ (67 mg, 0.1 mmol) was added. The resulting solution was stirred at room temperature for 6 h, after which the solvent was removed under vacuum. The KCl salt was precipitated in a CH$_2$Cl$_2$ solution and **4** crystallized by adding n-hexane. The orange precipitate (20 mg, 0.033 mmol, yield 33%) was filtered and characterized. It is completely soluble in in CH$_3$OH, CH$_3$CN, DMSO and CH$_3$Cl, it is partly soluble in H$_2$O and insoluble in hexane. Anal. Calcd. for C$_{31}$H$_{37}$ClO$_4$Ru: C, 61.02; H, 6.11. Found: C, 60.74; H, 6.20. mp: 230-232 °C. IR (cm^{-1}): 3296 mbr ν(-OH); 3012 w, 2955 w, 2923 w, 2857 w ν(aliphatic C-H); 1614 m ν(-C=O); 1574 sbr; 228 ν(Ru-Cl). ^{1}H-NMR (CD$_3$CN, 293 K): δ 1.98 (s, 18H, -(C*H*$_3$)$_6$ of hmb), 2.36 m, 2.44 m, 2.56 m (4H, C(3-3')*H*)), 2.82 (4H, C(4-4')*H*), 5.14 (s, 1H, C(1)*H*), 6.75 (d, 4H, C(7-7')*H*, ^{3}J$_{trans}$ = 8 Hz), 7.03 (m, 4H, (C-6-6')*H*). ^{13}C{^{1}H}-NMR (CD$_3$CN, 293 K): δ 14.28 (s, -(*C*H$_3$)$_6$ of hmb), 31.59 [s, C(4-4')], 42.21 [s, C(3-3')], 89.92 [s, C$_6$ of hmb], 97.34 (s, C1), 115.03 [s, C(7-7')], [s, C(6-6')], 132.61[s, C(5-5')], 155.16 [s, C(8-8')],

187.95 [s, C(2-2')=O]. ESI-MS (+) CH_3CN (m/z [relative intensity, %]): 575 [100] [Ru(hmb)(THbdcurc)]$^+$.

[Ru(benzene)(THbdcurc)Cl] (6)

THbdcurc (62 mg, 0.2 mmol) and KOH (11 mg, 0.2 mmol) were dissolved in CH_3OH (5 mL). After 1 h stirring at room temperature, [Ru(benzene)Cl_2]$_2$ (50 mg, 0.1 mmol) was added. The resulting solution was stirred at room temperature for 4 h, after which **6** formed and was filtered and dried. The orange precipitate (50 mg, 0.095 mmol, yield 95%) was characterized. It is completely soluble in in CH_3OH, CH_3CN, DMSO and CH_3Cl, it is partly soluble in H_2O and insoluble in hexane. Anal. Calcd. for $C_{25}H_{25}ClO_4Ru$: C, 57.09; H, 4.79. Found: C, 54.48; H, 4.74. mp: 206-207 °C. IR (cm^{-1}): 3345 mbr, 3179 mbr ν(-OH); 3072 w, 3051 w, 3038 w, 2967 w, 2933 w, 2910 w, 2852w ν(aliphatic C-H); 1612 m ν(-C=O); 1575 sbr; 259 ν(Ru-Cl).^{1}H-NMR (DMSO-d_6, 293 K): δ 2.33 (m, 4H, C(3-3')*H*)), 2.68 (4H, C(4-4')*H*), 5.14 (s, 1H, C(1)*H*), 5.59 (s, 6H, C_6H_6 of benzene), 6.68 (d, 4H, C(7-7')*H*, $^3J_{trans}$ = 8 Hz), 7.00 (d, 4H, (C-6-6')*H*). $^{13}C\{^1H\}$-NMR (DMSO-d_6, 293 K): δ 31.99 [s, C(4-4')], 42.29 [s, C(3-3')], 82.23 [s, C_6H_6 of benzene], 100.73 (s, C1), 115.43 [s, C(7-7')], 129.64 [s, C(6-6')], 131.79[s, C(5-5')], 155.92 [s, C(8-8')], 188.23 [s, C(2-2')=O]. ESI-MS (+) CH_3CN (m/z [relative intensity, %]): 491 [100] [Ru(benzene)(THbdcurc)]$^+$.

X-ray crystallography

A summary of the crystallographic data and the structure refinement results for compounds **2**-**4** is given in Table S6. Suitable crystals of were selected and mounted on an XtaLAB Synergy R, a

DW system, and a HyPix-Arc 150 diffractometer, where intensities were collected at 140 K using Cu Kα radiation. The datasets were reduced and corrected for absorption using *CrysAlis*^{Pro}.[32] The structure was solved with the ShelXT[33] solution program using dual methods and by using Olex2 1.5 as the graphical interface.[34] All non-hydrogen atoms were refined anisotropically using full-matrix least-squares based on $|F|^2$. Hydrogen atoms were placed at calculated positions using the 'riding' model. The CCDC numbers 2266740, 2266741 and 2266742 contain the crystallographic data for compounds **2**-**4**, respectively. These data can be obtained free of charge via www.ccdc.cam.ac.uk/data_request/cif.

Computational details

The electronic structure and geometries of the THcurcH and THbdcurcH proligands and their corresponding anions were calculated using density functional theory at the B3LYP level[35 36] with the 6-311G* basis set. Similarly, ruthenium complexes **1**-**6** (*closed* and *open* conformations) and the related complexes **7**-**12** were also calculated using DFT at the B3LYP level.[8] The Ru ion was described with the LANL2DZ basis set,[37] while the 6-31G* basis set was used for the other atoms. Molecular geometries of **2**-**4** were optimized starting from the crystallographic coordinates. Frequency calculations were carried out at the same level of theory to identify all of the stationary points as minima (zero imaginary frequencies). DFT calculations were performed using the Gaussian 09 suite of programs.[38] The computed IR spectra were scaled by a factor of 0.96.[39 40] The coordinates of all optimized compounds are reported in Table S7.

Cytotoxicity studies

The human ovarian cancer cell line A2780 and its cisplatin resistant form A2780cisR were purchased from the European Collection of Cell Cultures (ECACC, United Kingdom). The Human

Embryonic Kidney 293T cell line, HEK293T, was kindly provided by the BSF facility in EPFL. The media DMEM GlutaMAX and RPMI 1640 GlutaMAX were purchased from Life Technologies. The fetal bovine serum (FBS) was obtained from Sigma. A2780 and A2780cis cells were cultured in RPMI 1640 GlutaMAX, and HEK293T cells in DMEM GlutaMAX media containing 10% heat inactivated FBS at 37 °C and 5% CO2. To maintain resistance, the A2780cis cell line was routinely treated with cisplatin (2 μM) in the media. MCF-7 cells were grown in MEM supplemented with 10% FBS, 1% sodium pyruvate, antibiotic, and antimycotic; MCF-10A cells were cultured in a DMEM/F12 Ham's mixture supplemented with 5% equine serum, 20 ng/mL EGF, 10 μg/ mL insulin, 0.5 mg/mL hydrocortisone, antibiotics, and antimycotics. MCF-7CR cells were grown in minimum essential medium (MEM), 10% FBS supplemented with cisplatin 0.1 mg/mL, sodium pyruvate, antibiotics, and antimycotics. All these chemicals were cell culture grade and were obtained from Merck-Sigma. The cytotoxicity was determined using the MTT (3-(4,5-dimethyl-2-thiazolyl)-2,5-diphenyl2H-tetrazolium bromide) assay. The compounds were dissolved in DMSO and the resulting stock solutions were sequentially diluted in cell culture grade water to obtain a concentration range of 0–1 mM. 10 μL aliquots of these solutions were added in triplicates to a flat-bottomed 96-well plate. Subsequently, the cells were seeded in these plates as a suspension in the appropriate medium for each cell line (90 μL aliquots and approximately 1.4×10^4 cells/well), and the plates were incubated for 72 h. Cisplatin and RAPTA-C were used as positive and negative controls (0–100 μM), respectively. 10 μL of an MTT solution (5 mg/mL in Dulbecco's phosphate buffered saline) were added in each well, and the plates were incubated for 4 h at 37 °C. The medium was then carefully aspirated to conserve the purple formazan crystals, that were subsequently dissolved in 100 μL of DMSO/well. The absorbance of the resulting solutions, directly proportional to the number of surviving cells, was quantified at

590 nm using a SpectroMax M5e multimode microplate reader (using SoftMax Pro software, version 6.2.2). The data was analyzed with GraphPad Prism software (version 9.3.1). The percentage of surviving cells was calculated from the absorbance of wells corresponding to the untreated control cells (100%), and cell treated with 10 μM of gambogic acid (0%). The reported IC_{50} values are based on the means from three independent experiments, each comprising three tests per concentration level.

Fluorescence Anisotropy Measurements

Drug transport across cell membrane was monitored upon internalization of THcurcH, THbdcurcH and complexes **1**−**6** as described elsewhere.[28] Briefly, fluorescence anisotropy measurements were performed on an RF-5301PC Shimadzu spectrofluorometer at 37 °C using TMA−DPH probe (λ_{exc} = 340 nm; λ_{em} = 460 nm). MCF-7 cells (10^5/mL) were preincubated with 1 μM TMA−DPH and individually with 10 μM of the compound of interest. Polarized fluorescence data were recorded at 10 min intervals for 120 min, and fluorescence anisotropy (r) was calculated using the following model:

$$r = \frac{2\frac{I_{|}-I_{\perp}}{I_{|}+I_{\perp}}}{3-\frac{I_{|}-I_{\perp}}{I_{|}+I_{\perp}}} \qquad \text{Eq.1}$$

where $I_{|}$ and $I_{\perp}$ are the fluorescence intensities parallel and perpendicular to the excitation beam. The kinetic parameters for membrane entry and intracellular release (namely, k_{in} and k_{out}) were derived according to classic monoexponential models:

$$r_{in} = a(1 - e^{-k_{in}t}) + b \qquad \text{Eq.2}$$

$$r_{out} = c(e^{-k_{out}t}) + d \qquad \text{Eq.3}$$

Binding to DNA

The kinetics of binding of THcurcH, THbdcurcH and complexes **1**-**6** to DNA were evaluated using a biosensor-based assay.[41] Upon equilibration of the carboxylate surface of the sensor with PBS buffer (10 mM Na_2HPO_4, 2.7 mM KCl, 138 mM NaCl, pH = 7.4), a 5′-biotinylated ds-DNA oligomer (3′-CCACCCACTACCCTGGTTGGATGCTAATGT-5′) was blocked via streptavidin crosslinking as previously reported.[42] Next, each compound was independently added to the DNA-coated surface at different concentrations in the range of 0.6−6 μM, each time following binding kinetics up to equilibrium. Dissociation and regeneration steps were performed with fresh PBS buffer. The biosensor chamber was thermostatted at 37 °C throughout.

Immunometric quantification of p62/SQSTM1

The intracellular levels of p62/SQSTM1 were estimated by western blotting upon 24 h treatment of MCF-7 cells with 5 μM of complex **1** or THcurcH. Treated cells were lysed, and 15 μg of total proteins was separated by electrophoresis on 12% SDS-PAGE, then protein bands were electroblotted onto PVDF membranes (Millipore - Milan, Italy). After incubation with anti-p62/SQSTM1 monoclonal antibody (Merck Sigma - Milan, Italy), the immunodetections were carried out on a ChemiDoc™ MP imaging system (Bio-Rad - Milan, Italy). The gels were always loaded with molecular weight protein markers in the range of 6.5−205 kDa, and glyceraldehyde-3-phosphate dehydrogenase (GAPDH) was used as a control for equal protein loading. Western blot results were analyzed using ImageJ software.[43]

AUTHOR INFORMATION

Corresponding Author

*Riccardo Pettinari: riccardo.pettinari@unicam.it; tel. +39 0737402338.

Author Contributions

The manuscript was written through contributions of all authors. All authors have given approval to the final version of the manuscript. The authors declare no competing financial interest.

Conflicts of interest

There are no conflicts to declare.

Acknowledgements

The authors gratefully acknowledge funding from the European Union - Next-GenerationEU – National Recovery and Resilience Plan (NRRP) – MISSION 4 COMPONENT 2, INVESTMENT N. 1.1, CALL PRIN 2022 PNRR D.D. 1409 del 14-09-22 – (P20222TPZS, Theranostic Curcumin-Based Rare-Earth Agents) CUP N.J53D23014660001; The scholarship funded under NGEU – PNRR, DM 118/2023, M4 C1 I4.1 “ricerca PNRR”, CUP J11J23001330006. The Unione europea - FSE, Pon Ricerca e Innovazione 2014-2020; The Spanish Ministerio de Ciencia e Innovación (PGC2018-093443-B-I00). A.G. thanks Centro de Servicios de Informática y Redes de Comunicaciones (CSIRC), Universidad de Granada, for providing the computing time.

Supporting Information

The Supporting Information is available free of charge. It contains all the crystallographic details; the DFT calculations (i.e. optimized structures of ligands, proligands and complexes and MOs informations); monodimensional ^{1}H- and ^{13}C-NMR spectra and bidimensional {^{1}H-^{1}H}-COSY, {^{1}H-^{13}C}-HSQC, {^{1}H-^{13}C}-HMBC, {^{1}H-^{1}H}-NOESY NMR spectra; stability studies performed by ^{1}H-NMR and UV-Visible spectroscopy; anisotropy measurements and kinetic studies of binding to DNA.

ABBREVIATIONS

Curcumin (curcH), bisdesmethoxycurcumin (bdcurcH), tetrahydrocurcumin (THcurcH), bisdesmethoxytetrahydrocurcumin (THbdcurcH), CCR2, CC chemokine receptor 2; CCL2, CC chemokine ligand 2; CCR5, CC chemokine receptor 5.

REFERENCES

(1) Goel, A.; Kunnumakkara, A. B.; Aggarwal, B. B. Curcumin as "Curecumin": From Kitchen to Clinic. *Biochem. Pharmacol.* **2008**, *75* (4), 787–809.

(2) Priyadarsini, K. I. The Chemistry of Curcumin: From Extraction to Therapeutic Agent. *Molecules* **2014**, *19* (12), 20091 – 20112.

(3) Esatbeyoglu, T.; Huebbe, P.; Ernst, I. M. A.; Chin, D.; Wagner, A. E.; Rimbach, G. Curcumin — From Molecule to Biological Function Angewandte. *Angew. Chem. Int. Ed.* **2012**, *51*, 5308–5332.

(4) Salehi, B.; Stojanović-Radić, Z.; Matejić, J.; Sharifi-Rad, M.; Anil Kumar, N. V; Martins, N.; Sharifi-Rad, J. The Therapeutic Potential of Curcumin: A Review of Clinical Trials. *Eur. J. Med. Chem.* **2019**, *163*, 527–545.

(5) Dytrych, P.; Kejík, Z.; Hajduch, J.; Kaplánek, R.; Veselá, K.; Kučnirová, K.; Skaličková, M.; Venhauerová, A.; Hoskovec, D.; Martásek, P.; Jakubek, M. Therapeutic Potential and Limitations of Curcumin as Antimetastatic Agent. *Biomed. Pharmacother.* **2023**, *163*, 114758.

(6) Shabaninejad, Z.; Pourhanifeh, M. H.; Movahedpour, A.; Mottaghi, R.; Nickdasti, A.; Mortezapour, E.; Shafiee, A.; Hajighadimi, S.; Moradizarmehri, S.; Sadeghian, M.; Mousavi, S. M.; Mirzaei, H. Therapeutic Potentials of Curcumin in the Treatment of

Glioblstoma. *Eur. J. Med. Chem.* **2020**, *188*, 112040.

(7) Adeluola, A.; Zulfiker, A. H. M.; Brazeau, D.; Amin, A. R. M. R. Perspectives for Synthetic Curcumins in Chemoprevention and Treatment of Cancer: An Update with Promising Analogues. *Eur. J. Pharmacol.* **2021**, *906*, 174266.

(8) Prasad Sahdeo Tyagi Amit K., A. B. B. Recent Developments in Delivery, Bioavailability, Absorption and Metabolism of Curcumin: The Golden Pigment from Golden Spice. *Cancer Res Treat* **2014**, *46*, 2–18.

(9) Ireson, C. R.; Jones, D. J. L.; Orr, S.; Coughtrie, M. W. H.; Boocock, D. J.; Williams, M. L.; Farmer, P. B.; Steward, W. P.; Gescher, A. J. Metabolism of the Cancer Chemopreventive Agent Curcumin in Human and Rat Intestine. *Cancer Epidemiol. Biomarkers Prev.* **2002**, *11* (1), 105–111.

(10) Garcea, G.; Jones, D. J. L.; Singh, R.; Dennison, A. R.; Farmer, P. B.; Sharma, R. A.; Steward, W. P.; Gescher, A. J.; Berry, D. P. Detection of Curcumin and Its Metabolites in Hepatic Tissue and Portal Blood of Patients Following Oral Administration. *Br. J. Cancer* **2004**, *90* (5), 1011.

(11) Wang, K.; Qiu, F. Curcuminoid Metabolism and Its Contribution to the Pharmacological Effects. *Curr. Drug Metab.* **2013**, *14* (7), 791–806.

(12) Anand, P.; Kunnumakkara, A. B.; Newman, R. A.; Aggarwal, B. B. Bioavailability of Curcumin: Problems and Promises. *Mol. Pharm.* **2007**, *4* (6), 807–818.

(13) Lin, J. K.; Pan, M. H.; Lin-Shiau, S. Y. Recent Studies on the Biofunctions and

Biotransformations of Curcumin. *BioFactors* **2000**, *13* (1–4), 153–158.

(14) Wu, J. C.; Tsai, M. L.; Lai, C. S.; Wang, Y. J.; Ho, C. T.; Pan, M. H. Chemopreventative Effects of Tetrahydrocurcumin on Human Diseases. *Food Funct.* **2014**, *5* (1), 12–17.

(15) Aggarwal, B. B.; Deb, L.; Prasad, S. Curcumin Differs from Tetrahydrocurcumin for Molecular Targets, Signaling Pathways and Cellular Responses. *Molecules* **2015**, *20* (1), 185–205.

(16) Anand, P.; Thomas, S. G.; Kunnumakkara, A. B.; Sundaram, C.; Harikumar, K. B.; Sung, B.; Tharakan, S. T.; Misra, K.; Priyadarsini, I. K.; Rajasekharan, K. N.; Aggarwal, B. B. Biological Activities of Curcumin and Its Analogues (Congeners) Made by Man and Mother Nature. *Biochem. Pharmacol.* **2008**, *76* (11), 1590–1611.

(17) Pfeiffer, E.; Hoehle, S. I.; Walch, S. G.; Riess, A.; Sólyom, A. M.; Metzler, M. Curcuminoids Form Reactive Glucuronides in Vitro. *J. Agric. Food Chem.* **2007**, *55* (2), 538–544.

(18) Pettinari, R.; Marchetti, F.; Condello, F.; Pettinari, C.; Lupidi, G.; Scopelliti, R.; Mukhopadhyay, S.; Riedel, T.; Dyson, P. J. Ruthenium(II)-Arene RAPTA Type Complexes Containing Curcumin and Bisdemethoxycurcumin Display Potent and Selective Anticancer Activity. *Organometallics* **2014**, *33* (14), 3709–3715.

(19) Nakamura, Y.; Isobe, K.; Morita, H.; Yamazaki, S.; Kawaguchi, S. Metal Complexes Containing Acetylacetone as a Neutral Ligand. *Inorg. Chem.* **1972**, *11* (7), 1573–1578.

(20) Kharat, M.; Du, Z.; Zhang, G.; McClements, D. J. Physical and Chemical Stability of

Curcumin in Aqueous Solutions and Emulsions: Impact of PH, Temperature, and Molecular Environment. *J. Agric. Food Chem.* **2017**, *65* (8), 1525–1532.

(21) Wang, Y. J.; Pan, M. H.; Cheng, A. L.; Lin, L. I.; Ho, Y. S.; Hsieh, C. Y.; Lin, J. K. Stability of Curcumin in Buffer Solutions and Characterization of Its Degradation Products. *J. Pharm. Biomed. Anal.* **1997**, *15* (12), 1867–1876.

(22) Scolaro, C.; Hartinger, C. G.; Allardyce, C. S.; Keppler, B. K.; Dyson, P. J. Hydrolysis Study of the Bifunctional Antitumour Compound RAPTA-C, [Ru(g 6-p-Cymene)Cl 2 (Pta)]. *J. Inorg. Biochem.* **2008**, *102*, 1743–1748.

(23) Pettinari, R.; Petrini, A.; Marchetti, F.; Nicola, D. Influence of Functionalized H6-Arene Rings on Ruthenium(II) Curcuminoids Complexes. *ChemistrySelect* **2018**, *3*, 6696–6700.

(24) Aullón, G.; Bellamy, D.; Guy Orpen, A.; Brammer, L.; Eric A. Bruton. Metal-Bound Chlorine Often Accepts Hydrogen Bonds. *Chem. Commun.* **1998**, *6*, 653–654.

(25) Palmucci, J.; Marchetti, F.; Pettinari, R.; Pettinari, C.; Scopelliti, R.; Riedel, T.; Therrien, B.; Galindo, A.; Dyson, P. J. Synthesis, Structure, and Anticancer Activity of Arene-Ruthenium(II) Complexes with Acylpyrazolones Bearing Aliphatic Groups in the Acyl Moiety. *Inorg. Chem.* **2016**, *55* (22), 11770–11781.

(26) Marchetti, F.; Pettinari, R.; Di Nicola, C.; Pettinari, C.; Palmucci, J.; Scopelliti, R.; Riedel, T.; Therrien, B.; Galindo, A.; Dyson, P. J. Synthesis, Characterization and Cytotoxicity of Arene-Ruthenium(II) Complexes with Acylpyrazolones Functionalized with Aromatic Groups in the Acyl Moiety. *Dalt. Trans.* **2018**, *47* (3), 868–878.

(27) Chu, G. Cellular Responses to Cisplatin. The Roles of DNA-Binding Proteins and DNA Repair. *J. Biol. Chem.* **1994**, *269* (2), 787–790.

(28) Pagliaricci, N.; Pettinari, R.; Marchetti, F.; Pettinari, C.; Cappellacci, L.; Tombesi, A.; Cuccioloni, M.; Hadiji, M.; Dyson, P. J. Potent and Selective Anticancer Activity of Half-Sandwich Ruthenium and Osmium Complexes with Modified Curcuminoid Ligands. *Dalt. Trans.* **2022**, *51*, 13311–13321.

(29) Cuccioloni, M.; Bonfili, L.; Cecarini, V.; Nabissi, M.; Pettinari, R.; Marchetti, F.; Petrelli, R.; Cappellacci, L.; Angeletti, M.; Eleuteri, A. M. Exploring the Molecular Mechanisms Underlying the in Vitro Anticancer Effects of Multitarget-Directed Hydrazone Ruthenium(II)-Arene Complexes. **2020**, *15* (1), 105–113.

(30) Lei, C.; Zhao, B.; Liu, L.; Zeng, X.; Yu, Z.; Wang, X. Expression and Clinical Significance of P62 Protein in Colon Cancer. *Medicine (Baltimore).* **2020**, *99* (3).

(31) Liu, W. J.; Ye, L.; Huang, W. F.; Guo, L. J.; Xu, Z. G.; Wu, H. L.; Yang, C.; Liu, H. F. P62 Links the Autophagy Pathway and the Ubiqutin-Proteasome System upon Ubiquitinated Protein Degradation. *Cell. Mol. Biol. Lett.* **2016**, *21* (1), 1–14.

(32) CrysAlisPro Software System; Rigaku Oxford Diffraction; **2021**.

(33) Sheldrick, G. M. SHELXT - Integrated Space-Group and Crystal-Structure Determination. *Acta Crystallogr. Sect. A* **2015**, *71* (1), 3–8.

(34) Dolomanov, O. V; Bourhis, L. J.; Gildea, R. J.; Howard, J. A. K.; Puschmann, H. Olex2: A Complete Structure Solution, Refinement and Analysis Program. *J. Appl. Crystallogr.* **2009**,

42 (2), 339–341.

(35) Becke, A. D. Density-Functional Thermochemistry. III. The Role of Exact Exchange. , 98: 5648-5652. *J. Chem. Phys.* **1993**, *98*, 5648–5652.

(36) Lee, C.; Yang, W.; Parr, R. G. Development of the Colle-Salvetti Correlation-Energy Formula into a Functional of the Electron Density. *Phys. Rev. B* **1988**, *37* (2), 785–789.

(37) Hay, P. J.; Wadt, W. R. Ab Initio Effective Core Potentials for Molecular Calculations. Potentials for K to Au Including the Outermost Core Orbitals. *J. Chem. Phys.* **1985**, *82* (1), 299–310.

(38) Frisch, M. J.; Trucks, G. W.; Schlegel, H. B.; Scuseria, G. E.; Robb, M. A.; Cheeseman, J. R.; Scalmani, G.; Barone, V.; Petersson, G. A.; Nakatsuji, H.; Li, X.; Caricato, M.; Marenich, A.; Bloino, J.; Janesko, B. G.; Gomperts, R.; Mennucci, B.; Hratchian, H. P.; Ortiz, J. V.; Izmaylov, A. F.; Sonnenberg, J. L.; Williams-Young, D.; Ding, F.; Lipparini, F.; Egidi, F.; Goings, J.; Peng, B.; Petrone, A.; Henderson, T.; Ranasinghe, D.; Zakrzewski, V. G.; Gao, J.; Rega, N.; Zheng, G.; Liang, W.; Hada, M.; Ehara, M.; Toyota, K.; Fukuda, R.; Hasegawa, J.; Ishida, M.; Nakajima, T.; Honda, Y.; Kitao, O.; Nakai, H.; Vreven, T.; Throssell, K.; Montgomery, J. A. J.; Peralta, J. E.; Ogliaro, F.; Bearpark, M.; Heyd, J. J.; Brothers, E.; Kudin, K. N.; Staroverov, V. N.; Keith, T.; Kobayashi, R.; Normand, J.; Raghavachari, K.; Rendell, A.; Burant, J. C.; Iyengar, S. S.; Tomasi, J.; Cossi, M.; Millam, J. M.; Klene, M.; Adamo, C.; Cammi, R.; Ochterski, J. W.; Martin, R. L.; Morokuma, K.; Farkas, O.; Foresman, J. B.; Fox, D. J. Gaussian 09, Revision B.01. Gaussian, Inc. Wallingford CT, 2016.

(39) Wong, M. W. Vibrational Frequency Prediction Using Density Functional Theory. *Chem. Phys. Lett.* **1996**, *256* (4–5), 391–399.

(40) Scott, A. P.; Radom, L. Harmonic Vibrational Frequencies: An Evaluation of Hartree− Fock, Møller− Plesset, Quadratic Configuration Interaction, Density Functional Theory, and Semiempirical Scale Factors. *J. Phys. Chem.* **1996**, *100* (41), 16502–16513.

(41) Pettinari, R.; Pettinari, C.; Marchetti, F.; Skelton, B. W.; White, A. H.; Bon, L.; Cuccioloni, M.; Mozzicafreddo, M.; Cecarini, V.; Angeletti, M.; Nabissi, M.; Eleuteri, A. M. Arene − Ruthenium(II) Acylpyrazolonato Complexes: Apoptosis-Promoting E Ff Ects on Human Cancer Cells. *J. Med. Chem.* **2014**, *57*, 4532−4542.

(42) Cuccioloni, M.; Bonfili, L.; Cecarini, V.; Nabissi, M.; Pettinari, R.; Marchetti, F.; Petrelli, R.; Cappellacci, L.; Angeletti, M.; Eleuteri, A. M. Exploring the Molecular Mechanisms Underlying the in Vitro Anticancer Effects of Multitarget-Directed Hydrazone Ruthenium(II)–Arene Complexes. *ChemMedChem* **2020**, *15* (1), 105–113.

(43) Schneider, C. A.; Rasband, W. S.; Eliceiri, K. W. NIH Image to ImageJ: 25 Years of Image Analysis. *Nat. Methods* **2012**, *9*, 671–675.